Desiccation cracks on different substrates: simulation by a spring network model

2007 J. Phys.: Condens. Matter 19 356206

(http://iopscience.iop.org/0953-8984/19/35/356206)

IOP PUBLISHING JOURNAL OF PHYSICS: CONDENSED MATTER

J. Phys.: Condens. Matter **19** (2007) 356206 (10pp) doi:10.1088/0953-8984/19/35/356206

Desiccation cracks on different substrates: simulation by a spring network model

Supti Sadhukhan[1], Shashwati Roy Majumder[2], Dibyendu Mal[1], Tapati Dutta[3] and Sujata Tarafdar[1]

[1] Condensed Matter Physics Research Centre, Physics Department, Jadavpur University, Kolkata 700032, India
[2] Theoretical Chemistry Section, Chemistry Group, Bhabha Atomic Research Centre, Trombay, Mumbai 400085, India
[3] Physics Department, St Xavier's College, Kolkata 700016, India

Received 14 May 2007, in final form 26 June 2007
Published 2 August 2007
Online at stacks.iop.org/JPhysCM/19/356206

Abstract

Crack patterns formed due to desiccation of clay or similar materials show distinctive reproducible patterns. If one measures the cumulative area $A_{\rm cum}$ covered by the cracks with widths $\geqslant W_{\rm min}$, then $A_{\rm cum}$ plotted against $W_{\rm min}$ shows a typical reproducible shape. In a log–log plot, this curve has two roughly linear regions with different slopes. For a polypropylene (PP) substrate, there is a sharp change from a nearly horizontal line to a very steep line, whereas for a glass substrate, which is smoother, there is a gradual changeover between the two regions. We propose a simple one-dimensional spring chain model, in which reducing the natural length of the springs corresponds to the desiccation process. Springs may break, or slip against the substrate to accommodate strain beyond a specified threshold. The model successfully reproduces the successive stages of crack formation and behaviour of the cumulative area curve, as observed in experiments. The difference in the qualitative nature of the patterns on smooth and rougher substrates is also obtained.

1. Introduction

Crack patterns in drying clay films have a distinctive hierarchical structure; this has been discussed in several earlier papers [1–7]. Different aspects of the problem have been investigated by different groups. Bohn *et al* [4] studied the hierarchical order of appearance of the cracks leading to a network with three-fold vertices. They suggested a method for quantitative characterization of the pattern, as did Vogel *et al* [8] through topological tools, such as Minkowski numbers. The dynamical aspect of crack development in time was studied in [5] and [8]. Lecocq and Vandewalle [5] studied the effect of the drying rate on crack widths and spacing. Pauchard *et al* [9] studied the variation in crack patterns on a drying drop of colloidal suspension, as the salt concentration is changed. Groisman and Kaplan [3] demonstrate that

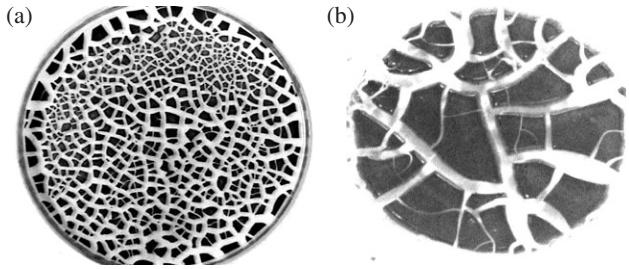

Figure 1. Cracks formed in desiccated layers of laponite–methanol suspension on (a) PP substrate and (b) glass substrate. The circular Petri dishes are 10 cm in diameter.

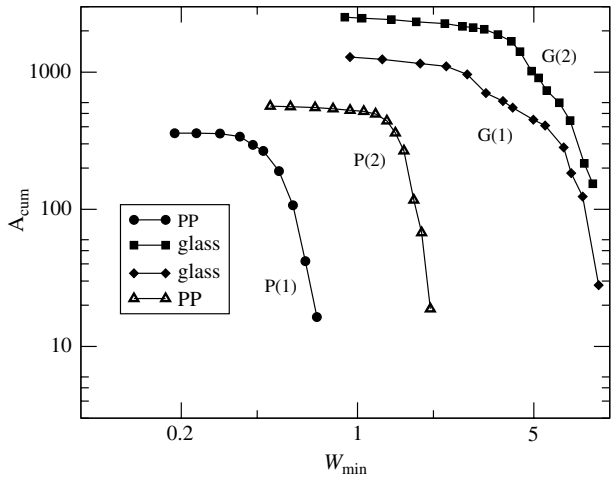

Figure 2. The area A_{cum} covered by cracks of width $\geqslant W_{min}$. There is a sharp knee for the PP samples, but the curves for glass are gently sloping. The curves P(1) and G(1) represent samples with less thickness on PP and glass respectively, and P(2) and G(2) are for thicker layers; the other experimental conditions are the same as those given in the text.

in many cases cracking is due to the friction between the substrate and the drying suspension; moreover, the linear size of the crack patterns scales with film thickness.

The problem of cracking in desiccating clay has an impact in the field of geology as well; this has been emphasized in many papers [10–12]. Reference [10] is an experimental study on a system to mimic desiccation cracks in clay liners of water channels. Reference [12] reports the formation of sorted polygonal structures in clay when glaciers recede.

Computer simulations of the problem have been done as well, e.g. [13–17]. Other interesting ramifications are the effect of memory of vibrations in crack formation [18] and the effect of a static electric field imposing pattern selection [19]. Earlier work on laponite [1, 20, 21] reported very characteristic fractal patterns on different substrates, as shown in figure 1. The cumulative area covered by the cracks when observed under successively decreasing resolution gives a typical nature in a log–log plot [1, 20]. Experimental results for PP and glass substrate are shown in figure 2. Here the area covered by cracks of width $\geqslant W_{min}$ is plotted against W_{min}. The curves have an almost horizontal part at higher resolution (towards the left) and a knee followed by a fall at low resolution. For a smooth substrate like glass, the fall is relatively gentle, whereas for the rougher PP, the fall is very steep.

The present work reports experimental results for crack patterns for drying laponite–methanol suspensions on PP and glass substrates. We develop a spring network model of the layer and use it to simulate the drying process. We show that this model can reproduce the typical shape of the curves in figure 2. The difference in the qualitative nature of the curves on different substrates is also reproduced. The present model is one-dimensional, so the initial sample is represented by a line of a certain length. This picture corresponds to a vertical section of a real thin layer in the experiment. As the cracks form, the line breaks up into smaller pieces, separated by gaps, which represent the crack width. The experiment is done on a three-dimensional system, but since we look at the surface, the analysis is effectively two-dimensional. When comparing with experiments, the cumulative crack *area* in the experiment is replaced here by the cumulative crack *width*.

Section 2 gives the experimental procedure and results in brief; details for the PP substrate experiment are to be found in [1, 20]. Section 3 discusses the spring chain model in detail. Results from the simulation are compared with experimental results in section 4.

2. The experiment

2.1. Procedure

The experiment was performed in PP and glass Petri dishes of diameter 10 cm. The films were prepared as follows: laponite(RD) was mixed with methanol and stirred in a magnetic stirrer for 1 h to make a suspension. A pinch of dye was added to each of the samples. This does not affect the crack patterns but enhances clarity. The mixture was poured into a Petri dish and allowed to dry at room temperature. The temperature during the experiment was between 32 and 36 °C and the humidity was in the range 76%–78%. As the methanol evaporated, it was observed that the crack patterns started to develop after about one to two days. The whole crack pattern was photographed by a CCD camera at intervals as it formed.

2.2. Results

Figure 1 shows crack patterns on PP and glass substrates respectively. On PP (A) the cracks are numerous and narrow; on glass (B) a lesser number of wider cracks are seen. The cumulative area covered by the cracks for widths $\geqslant W_{\min}$ is plotted against increasing $W_{\min}$, which corresponds to lower resolution. The curves given for PP and glass in figure 2 show that, for PP, the curve falls off much more sharply than for glass.

3. The spring chain model

3.1. Description of the system

We represent the thin layer of clay suspension by a chain of nodes a, b, c, d,... connected by horizontal springs with spring constant S_{h} (figure 3) to each other and by vertical springs, with spring constant S_{v}, to the nodes A, B, C, D,... on the substrate. The spring constants are taken as $S_{\mathrm{h}} = S_{\mathrm{v}} = 1$.

Initially all springs have a natural length $d_0 = 1$ and the vertical springs are perfectly vertical. The nodes a, b, c, d,... and A, B, C, D,... lie on a unit lattice. The drying process is represented by a reduction in the natural (unstrained) length of all the horizontal springs. The nodes a, b, c,... are allowed to move horizontally, but not vertically, to accommodate the stress generated.

As the stress builds up, two things can happen: (1) a 'break' or (2) a 'slip'. If the strain in the horizontal springs exceeds a threshold H_{th}, the spring breaks, and a crack starts to form. As

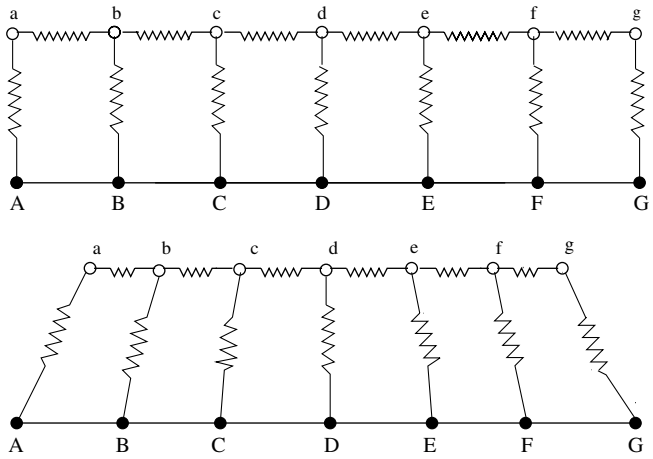

Figure 3. The initial configuration of the spring chain is shown in the upper figure and the configuration after one step of desiccation in the lower figure. The nodes a, b, c,... are connected by the horizontal springs to each other, and by vertical springs to the nodes A, B, C,... on the substrate.

the nodes shift horizontally, the vertical springs are no longer vertical; they form an angle to the horizontal, and if stretched beyond a threshold V_{th}, the lower node on the substrate slips until the position corresponding to maximum permissible strain is regained. The vertical springs are not allowed to break.

The desiccation occurs in steps; at the $(n + 1)$th step, the natural length is reduced by a fraction of the length at the nth step. So the drying rate is a function of time, decreasing with time according to a power law.

After one desiccation step, the energy of the system is minimized by the conjugate gradient method [22] and the nodes a, b, c,... are allowed to relax to their minimum energy position. It is then checked whether the strain in any of the springs exceeds the breaking or slipping limit; if so, the necessary break and/or slip is implemented, and the energy minimization procedure is re-run, until an equilibrium is reached. The widths and positions of the cracks at equilibrium are noted. The rate of desiccation decreases with time, so eventually the system stabilizes, and we now consider the system to be completely dry.

The successive cracks appear as shown schematically in figure 4. However, though no disorder is explicitly introduced, the inherent noise due to rounding-off errors makes the system lose perfect symmetry after a few stages.

The widths of all cracks at the final stage are noted, and the cumulative length L_{cum} of the system covered by cracks with width $\geqslant W_{\text{min}}$ is computed. Decreasing W_{min} corresponds to observing the system under higher and higher resolution. When L_{cum} for cracks with width $\geqslant W_{\text{min}}$ is plotted against W_{min}, a curve is obtained, with the same typical shape seen in the experimental results [1, 20]. In the experiment the cumulative *area* covered by the cracks was measured. For the present one-dimensional simulation we consider this to be equivalent to the cumulative width.

3.2. Details of the simulation

The length of the chains are taken as 100 units. Initially, all the adjacent nodes are at unit distance from each other. The springs are supposed to be in their relaxed position in this

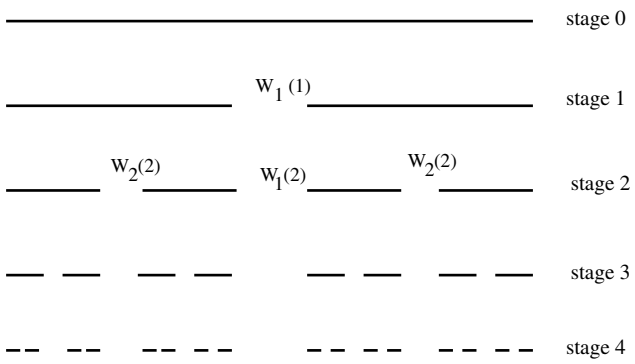

Figure 4. The successive stages of crack formation are shown schematically. We show the appearance of the film at the mth stage with the width $W_i(m)$ of the crack formed at the ith time step.

configuration. The lower chain of nodal points A, B, C, D,... is supposed to be attached to the substrate. The upper chain a, b, c, d,... represents the substance which undergoes desiccation. Both S_h and S_v have been assigned unit value. To bring about the effect of desiccation in our simulation, the length of each link in the upper chain is reduced according to the rule

$$d_{n+1} = d_n(1 - b/r^n), \tag{1}$$

where d_{n+1} and d_n represent the natural length between two nodes in the $(n + 1)$th and nth time step, b is a constant and r is a parameter which controls the rate of decrease in the natural length from one time step to the next higher time step. The value of b is kept constant at 0.1, and initial time corresponds to $n = 0$.

The rate of desiccation should reduce with time; this has been incorporated through the power law. After a certain time step n_sat, there is no further significant decrease in the length and the natural length saturates. Keeping the centre of the chain undisturbed, the left and right halves shrink symmetrically. If x_0 and $x_i(n)$ represent the centre position and any nodal position respectively at a time step n, then the new nodal position in the next time step can be written as

$$x_i(n + 1) - x_0 = (1 - b/r^n)(x_i(n) - x_0). \tag{2}$$

This configuration may not be the minimum potential energy configuration of the system. The system now relaxes to the minimum energy configuration, implemented through the conjugate gradient method [22]. The positions of the N nodes of the upper chain as a whole may be represented by a single point P, in an N-dimensional space. The function $f(P)$ returns the sum of the potential energies of all springs. This potential energy arises due to the change in length of the spring as a result of desiccation, and is given by

$$f(P) = \Sigma \tfrac{1}{2} S_\mathrm{h} \delta d^2. \tag{3}$$

A similar expression with S_v replacing S_h will give the total potential energy for the vertical springs.

The function $\mathrm{d}f(P, \nabla_j)$ returns the gradient of the function $f(P)$ evaluated at the point P, where j denotes any of the coordinate axes. The gradient information from function $\mathrm{d}f(P, \nabla_j)$ is used to choose the directions along which we should proceed to determine the location of P for minimum potential energy.

The Fletcher–Reenes–Polak–Ribiera minimization (which employs the conjugate gradient algorithm) is performed on the function $f(P)$ to obtain the new location of P [22]. In the

configuration obtained after minimization of 'potential energy' the vertical springs are found to be stretched more as we proceed from the centre of the system towards the extremities. In contrast, the horizontal springs are stretched more towards the centre of the chain. A maximum permissible limit $H_{\rm th}$ has been set for the strain in each horizontal spring. There can be more than one spring whose strain is greater than the maximum limit set. But at any one time instant, only a single spring is allowed to break [23, 13]. The spring with the maximum strain is then broken and the network splits into two. There is no breaking limit set for the vertical springs. Instead a provision is kept for slipping of the lower nodal points to release the excess strain so that it is just equal to the maximum permissible strain. The node may be shifted right or left depending on the angle made by the corresponding spring with the positive x-axis being acute and obtuse respectively.

If the upper chain breaks (which may be accompanied by slipping) then the daughter networks are indexed such that their hierarchy can be traced. These two individual networks undergo the minimization process separately. If there is only slipping then the conjugate gradient method is also applied on it to obtain the minimum energy location. The condition for slipping and/or splitting is rechecked. If it splits, these two are treated as two different networks, else the process of finding the minimum energy location continues until there is no more slipping. If the natural length (at that time instant) of the spring in the upper chain of the concerned network is equal to the saturated length, no further desiccation is done. If not, then the next time step desiccation is applied on the concerned networks according to equation (1). Finally when all the sub-networks have reached the saturated point individually, the gaps are calculated between the nodes where the springs have broken. These gaps represent the final crack widths, as illustrated in figure 4. This schematic diagram simply demonstrates the generation of the daughters in hierarchical stages, and shows that the number of sections grows in a power law, as in a cantor set. However, in the present work we are concerned with the distribution of crack widths, i.e. the gaps between the segments. This is obtained from the simulation algorithm described here.

3.3. Simulation results

In the present study the parameters $S_{\rm h}$, $S_{\rm v}$ and b are kept constant. Then the parameters controlling the crack formation process are $H_{\rm th}$, $V_{\rm th}$ and r, which represent respectively, the breaking threshold (for horizontal springs), the slipping threshold (for vertical springs) and the power-law exponent controlling the desiccation rate. These parameters are varied one by one. The results for the sets of parameters which give realistic $A_{\rm cum}$ versus $W_{\rm min}$ curves are discussed below.

Experimentally, the area covered by the solid shrinks to about 70% of the initial area on desiccation. We set the value of r to get a realistic reduction in the solid area, which is between 30 and 40% of the initial sample length. This range of r lies between 1.2 and 1.3. In most of the cases the total number of cracks up to saturation was in the range 30–40. These are binned in convenient ranges of δW from 0.001 to 0.02, to get around ten points representing the cumulative crack width. For some specific combinations of parameters, the number of cracks is very low—about 10–15; we do not analyse these cases. $L_{\rm cum}$ is plotted against $W_{\rm min}$ for different parameters in figures 5 and 7.

In the first set, there was no slipping allowed. $H_{\rm th}$ was increased from 0.01 onwards for three values of r—1.2, 1.25 and 1.3. No marked difference was observed for the different rs. We found that, for each r, there is a maximum limiting value for $H_{\rm th}$ for which cracks appear. These values are respectively 0.66, 0.5 and 0.4 for $r = 1.2$, 1.25 and 1.3, irrespective of $V_{\rm th}$. Figure 5 shows that wider cracks are obtained for higher values of $H_{\rm th}$. In addition, the number of cracks decreases with increasing $H_{\rm th}$, but the decrease is not monotonic.

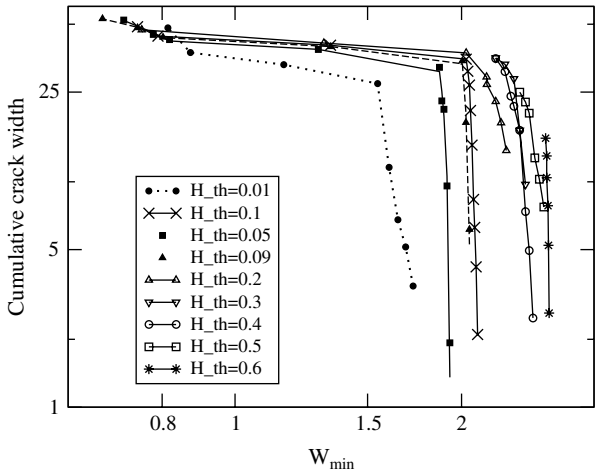

Figure 5. Simulation results for cumulative crack width for widths $\geqslant W_{\min}$, when no slipping is allowed on the substrate. The lines are guides to the eye.

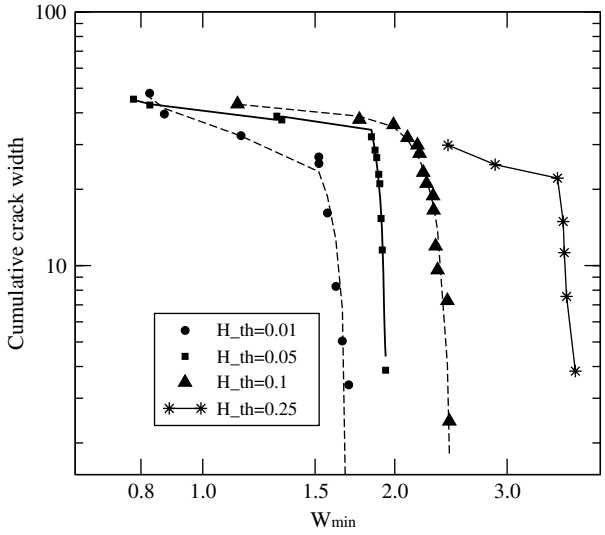

Figure 6. Simulation results for cumulative crack width for widths $\geqslant W_{\min}$, with slipping threshold $V_{\text{th}} = 0.08$ and $r = 1.25$. The lines are guides to the eye. The effect of varying the breaking threshold is shown.

In the second set, we varied V_{th} from 0.01 onwards and for each value, studied the effect of variation of H_{th} and r. Here again the nature of the patterns observed were similar for different r. Figure 6 shows a typical graph obtained for V_{th} fixed at 0.08 and r fixed at 1.25. Wider cracks appear for higher H_{th} values.

In the third set, we observe the change with variation of V_{th}. We fixed H_{th} and varied V_{th} from 0.005 upwards. It was found that, for a given H_{th}, there is an upper limit to V_{th}, beyond which the crack pattern does not change. Moreover, this upper limit increases with increasing H_{th}. Figure 7 shows the pattern obtained for H_{th} fixed at 0.01. Here we observe that for low V_{th}, say 0.005, the nature of the pattern is different from that obtained for higher values. For low V_{th},

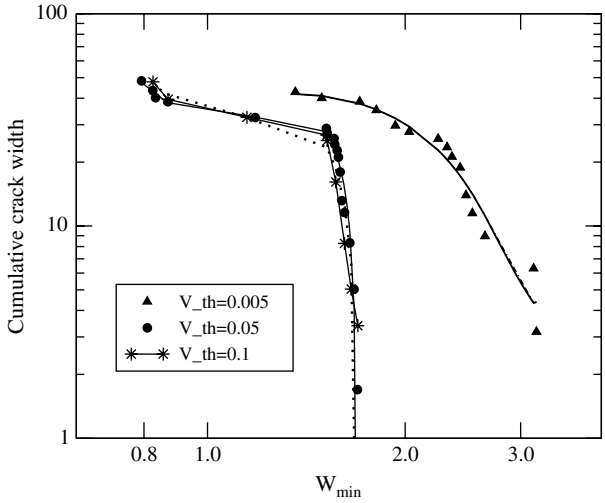

Figure 7. Simulation results for cumulative crack width for widths $\geqslant W_{\min}$, with breaking threshold $H_{\text{th}} = 0.01$ and $r = 1.25$. The effect of varying the slipping threshold is shown.

the curve for cumulative crack width is gently sloping from an almost horizontal line at small $W_{\min}$ to a moderate negative gradient. On increasing V_{th}, the curve has a sharper crossover from the horizontal and the larger $W_{\min}$ side becomes steeper, until above $V_{\text{th}} \sim 0.08$ there is hardly any change on further increase of V_{th}. Low V_{th} implies that the sample slips easily along the substrate,i.e. the substrate has a smoother texture.

4. Discussion

It is clear that the spring chain model, in spite of its simplicity, reproduces the crack formation process quite well. The split near the centre of the sample producing the widest crack and subsequent splittings of the daughters in successive stages are all well reproduced. The A_{cum} versus $W_{\min}$ curves look remarkably similar to the experimental curves for the right set of parameters. The position of the knee of the curve W_{th}, with respect to the maximum crack width obtained $W_{\max}$, i.e. the extreme point on the right for each simulation, is a characteristic of the cracking process. The ratio $W_{\text{th}}/W_{\max}$ was found to be near 0.7 in the experiments on PP [20]. In the simulation the knee point lies in the range 0.74–0.95. There is no definite knee point for the case with lower V_{th}, which mimics the glass substrate. If we consider the intersection of the two linear regions as the knee point in this case, then the ratio $W_{\text{th}}/W_{\max}$ is around 0.6 in the experiments and 0.68 in the curve shown in figure 7.

With the slipping condition completely suppressed, the steep part of the curve looks unrealistically near-vertical. Inclusion of V_{th} gives more realistic rounded knee. Reducing V_{th} to make the substrate more slippery produces exactly the change in the nature of the curve we get when changing the substrate from PP to glass. Glass is of course much smoother than a polymer substrate [24] as revealed by scanning electron microscopy study. No slip also implies that the cracks form at the surface only, and do not reach the substrate; this is also unrealistic. Comparison of figures 2 and 7 shows that the simulation curves for a rough and smooth substrate reproduce the experimental situation very well.

The breaking threshold H_{th} for the horizontal springs are representative of the cohesive bonding between particles of the material itself. It is expected to be related to the breaking

stress of the desiccating layer. The spring constants S_h and S_v, which we have not varied in the present study, should be related to the elastic properties of the layer and possibly other physical parameters of the suspension, such as the viscosity. We plan to vary the desiccating material and see if variation of H_{th} and spring constants in the simulation can be related to its properties.

Though our model is one-dimensional, the results for cumulative linear coverage of the cracks agree quite well with the surface crack coverage in the real system. The reason is that the real system is isotropic, and the cumulative crack area and cumulative crack length scale similarly with crack width. Hence, in a log–log plot, the curves for linear coverage, in a vertical section and for areal coverage on the surface, are similar in nature, only with a vertical shift.

The model employed here is somewhat similar to the model of [13, 15], but this model was not used to calculate the area covered by cracks. Leung and Neda [13] have proposed a spring block model, which demonstrates scaling of the crack pattern with layer thickness. Vogel *et al* [17] develop a two-dimensional spring network model on a triangular lattice to mimic the topological features observed in the experimental results in [8]. Other simulation models include numerical work in [15] which show finger-like instabilities in crack development, which show a limiting behaviour analogous to Laplacian growth models.

In [21] a phenomenological model was proposed which explained the steeper power-law region in figure 2. Here successive divisions of the initial sample was assumed to follow an ad hoc rule, with the crack width decreasing by a constant factor at each stage. The more realistic spring model presented here is able to reproduce the entire curve quite well. This model has been developed along the lines of spring models employed by [25, 26], but with considerable departure so as to suit the present problem.

In figure 2 the two curves with PP and two with glass represent films with different thicknesses. The thicker layer has wider cracks for both types of substrate. The effect of thickness has not been incorporated in the present one-dimensional model; we plan to extend the model to at least two dimensions in future.

Acknowledgments

SRM gratefully acknowledges financial support from the Department of Science and Technology, New Delhi (Fellowship No: SR/WOS-A/CS-52/2003). The authors are very grateful to T K Ballabh for helpful suggestions regarding the computer simulation. Suparna Sinha is acknowledged for help in experiments and valuable discussion.

References

[1] Mal D, Sinha S, Mitra S and Tarafdar S 2005 *Physica* A **346** 110–5
[2] Shorlin K A and de Bruyn J R 2000 *Phys. Rev.* E **61** 6950–7
[3] Groisman A and Kaplan E 1994 *Europhys. Lett.* **25** 415
[4] Bohn S, Platkiewicz J, Androetti B, Adda-Bedia M and Couder Y 2005 *Phys. Rev.* E **71** 046215
[5] Lecocq N and Vandewalle N 2003 *Physica* A **321** 431
[6] Allain C and Limat L 1995 *Phys. Rev. Lett.* **74** 2981
[7] Komatsu T S and Sasa S 1997 *Japan. J. Appl. Phys.* **36** 391
[8] Vogel H J, Hoffmann H and Roth K 2005 *Geoderma* **125** 203
[9] Pauchard L, Parisse F and Allain C 1999 *Phys. Rev.* E **59** 3737
[10] Miller C J, Mi H and Yesiller N 1998 *J. Am. Water. Resources Assoc.* **34** 677
[11] Ayad R, Konrad J M and Soulie M 1997 *Can. Geotech. J.* **34** 929
[12] Ballantyne C K and Matthews J A 1983 *Arctic Alpine Res.* **15** 339
[13] Leung K and Neda Z 2000 *Phys. Rev. Lett.* **85** 662–5
[14] Kitsunezaki S 1999 *Phys. Rev.* E **60** 6449
[15] Kitsunezaki S 2004 *Gran. Matter* **6** 221

[16] Malthe-Sorenssen A, Jamtveit B and Meakin P 2006 *Phys. Rev. Lett.* **96** 245501
[17] Vogel H J, Hoffmann H, Leopold A and Roth K 2005 *Geoderma* **125** 213
[18] Nakahara A and Matso Y 2006 *Phys. Rev.* E **74** 045102(R)
[19] Mal D, Sinha S, Middya T R and Tarafdar S 2007 *Appl. Clay Sci.* at press doi:10.1016/j.clay.2007.05.005
[20] Mal D, Sinha S, Mitra S and Tarafdar S 2006 *Fractals* **14** 283–8
[21] Mal D, Sinha S, Dutta T, Mitra S and Tarafdar S 2007 *J. Phys. Soc. Japan* **76** 014801
[22] Press W H, Teukolsky S A, Vetterling W T and Flannery B P 1986 *Numerical Recipies in Fortran F77: The Art of Scientific Computing* (Cambridge: Cambridge University Press)
[23] Hayakawa Y 1994 *Phys. Rev.* E **49** R1804
[24] Sinha S 2007 private communication
[25] Majumder S R, Bandhyopadhyay T and Ghosh S K 2005 *Radiat. Phys. Chem.* **74** 252–60
[26] Gunaratne G H, Rajapaksa C S, Basser K E, Mohanty K K and Wimalawansa S J 2002 *Phys. Rev. Lett.* **88** 068101